ORGANOMETALLICS

Article

Cite This: *Organometallics* XXXX, XXX, XXX−XXX

pubs.acs.org/Organometallics

Mechanistic Studies on the Nickel-Catalyzed Cyclopropanation with Lithiomethyltrimethylammonium Triflate

Stefan A. Künzi, Renana Gershoni-Poranne, and Peter Chen*

Laboratorium für Organische Chemie, ETH Zürich, CH-8093 Zürich, Switzerland

Supporting Information

ABSTRACT: We report here our mechanistic study of the previously published nickel-catalyzed cyclopropanation reaction using lithiomethyltrimethylammonium triflate as methylene donor. The cyclopropane yield is highly dependent on the olefin substrate and correlates well with the binding affinity of the olefin to Ni(0) as established elsewhere. On the basis of this observation, we developed a simplified mechanistic model that can explain several odd observations we found in our initial report. Most importantly, a binding equilibrium between the olefin substrate and phosphine ligand appears to govern the ratio between product formation and unproductive ylide decomposition in a side reaction.

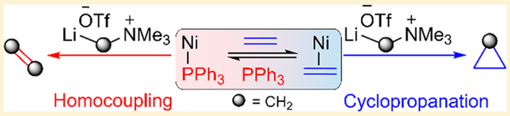

Downloaded via UNIV AUTONOMA DE COAHUILA on May 2, 2019 at 22:44:29 (UTC).
See https://pubs.acs.org/sharingguidelines for options on how to legitimately share published articles.

1. INTRODUCTION

Only a few methods are known for transferring methylene to electron-rich alkenes to form cyclopropanes. For large scale production, the Simmons−Smith and related metal carbenoid-based reactions are preferred, though they often suffer from the generation of large amounts of waste.[1] Transition-metal-catalyzed cyclopropanation using diazomethane is a well-studied and very versatile method, but, due to the inherent instability and toxicity of the reagent itself, or its precursors, the reaction is limited to small-scale reactions.[2]

To circumvent these drawbacks, extensive research had focused on the in situ generation of diazomethane from more stable precursors, in order to circumvent the need for isolation or the design of new reagents as methylene donors.[3]

Recently, we took the alternative approach of non-diazo methylene donors and reported on the nickel-catalyzed cyclopropanation of several electron-rich, alkyl substituted alkenes using lithiomethyltrimethylammonium triflate as methylene donor, generated in situ from tetramethylammonium triflate and BuLi (Scheme 1).[4]

In that report, we also noted a peculiar behavior with respect to the catalyst loading. The highest yield of cyclopropanation of cyclooctene (COE) was obtained with a catalyst loading in the range of 0.5−1.0 mol %. At lower or higher loadings, a decreased yield was obtained, resulting in a bell-shaped curve for catalyst loading versus yield. We observed polyethylene and small amounts of cyclopropane (C_3H_6) as side products, presumably stemming from initial formation of ethene via homocoupling of two nickel carbenes.

We proposed an explanation based on two competing processes with the same intermediate species, i.e., a nickel carbene that can undergo either cyclopropanation with an alkene to afford the cyclopropane product or homocoupling with another nickel carbene molecule to afford ethene. The initially formed ethene could then react further, to afford the observed side products. Overall, this would lead to an unproductive decomposition of the reagent. We predicted the product formation to be kinetically first-order in catalyst and the homocoupling to be second-order (assuming the homocoupling step to be rate-limiting, rather than nickel carbene formation) or at least bimolecular with respect to the proposed nickel carbene. Overlaying these two competing reactions could then explain the observed behavior, where the

Scheme 1. Previously Reported Cyclopropanation Using Tetramethylammonium Triflate as Methylene Donor and a Proposed Simplified Catalytic Cycle[4]

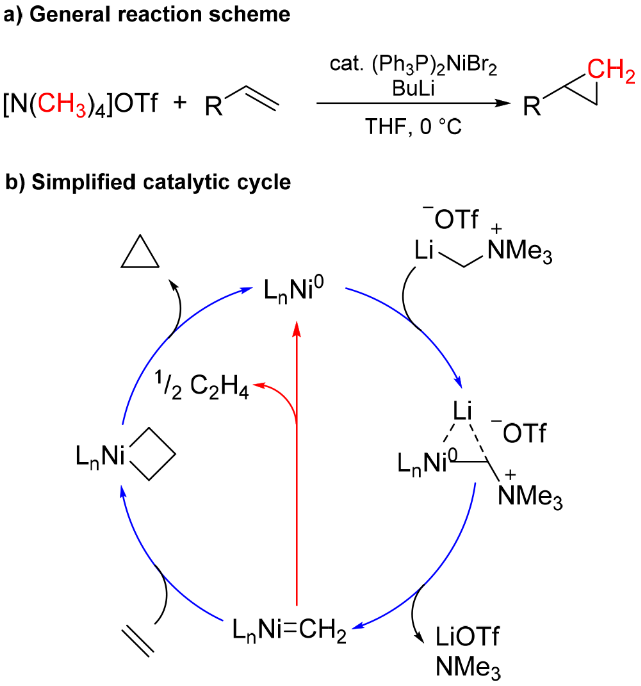

Received: January 18, 2019

homocoupling kinetically outcompetes product formation at high catalyst loadings, at least for the reported case of catalyst loadings above the optimum 0.5−1 mol % with $(Ph_3P)_2NiBr_2$ as precatalyst and COE as substrate.

Additionally, we observed that the yield was influenced by whether the flask was open or closed to an argon Schlenk line, when using COE as substrate.[5] On the basis of these and other experimental observations, and in analogy to literature precedent of isolated nickel species, we postulated a possible catalytic cycle with a nickel carbene as an important intermediate.[6]

Herein, we report mechanistic studies, including extensive kinetic and computational investigations, which support the involvement of a reactive nickel carbene intermediate, and reveal the intricate balance between ligand and alkene binding that explains the observed substrate dependence of the cyclopropanation yield.

The rationale for this work is formulated as the following series of questions, which we seek to address herein.

Firstly, what is the possible resting state of the catalyst? What are the ligands bound to the nickel?

Secondly, what is the cause of the substrate dependence that we noticed earlier? How does the substrate dependence relate to the catalyst resting state?

Thirdly, what causes the effect of the catalyst loading on the cyclopropanation yield?

Fourthly, why is there a difference between running the reaction open or closed to the argon Schlenk line?

The findings we report here help us to formulate an answer as to what might be the catalyst resting state and how this relates to the π-acidity and formation constant of the π-complex of the substrate with the catalyst. The resultant model we propose, albeit rather simple, offers an explanation to the aforementioned effect on catalyst loading. Alkene competition experiments within this model framework offer insights regarding the reactivity and stability of the resting state.

2. EXPERIMENTAL METHODS

Kinetic measurements were conducted by quenching aliquots under protic conditions. Product formation was measured by GC-FID using a previously added internal standard, and k_{obs} was determined using initial rates.

The consumption of ylide was measured indirectly by determining the relative amount of remaining $[NMe_4]^+$ by ^1H NMR against a previously added internal standard. An exponential fit over the entire reaction profile was used to determine k_{obs}.

We used two different Methods, A and B, that differ in the generation of the ammonium ylide reagent, either in situ (A) or preformed (B) (see Scheme 2).

For method A, $[NMe_4]OTf$ (1.1 equiv), alkene, and catalyst were mixed together, cooled to 0 °C; then BuLi (1 equiv) was added to form the ylide in situ.

For method B, the ammonium salt was deprotonated first (in the *presence or absence of alkene*) before the catalyst was added to the preformed ylide to initiate the cyclopropanation/ylide decomposition.

2.1. Computations. All calculations were performed using Gaussian 09, Revision D.[7] All geometries were optimized, and frequencies calculations were performed to ensure real minima for the intermediates (i.e., $N_{imag} = 0$) and first-order saddle points for the transition states (i.e., $N_{imag} = 1$). The energies reported are zero-point corrected energies. We first performed a benchmarking procedure, in which we compared crystal structures of literature-reported compounds that are analogous to the intermediates in our system to computationally optimized structures (19 different combinations of density functionals and basis sets were tested; Table S20 summarizing the results is provided in the Supporting Information (SI)). Following this procedure, we settled on the functional/basis-set combination M06L/def2-SVP, and these results are presented in the text. In addition, we performed calculations at the same level with an implicit solvent model, which yielded similar results.

Scheme 2. Two Different Methods Employed To Generate the Active Reagent $[LiCH_2NMe_3]OTf$, Either after (A) or before (B) Addition of Catalyst

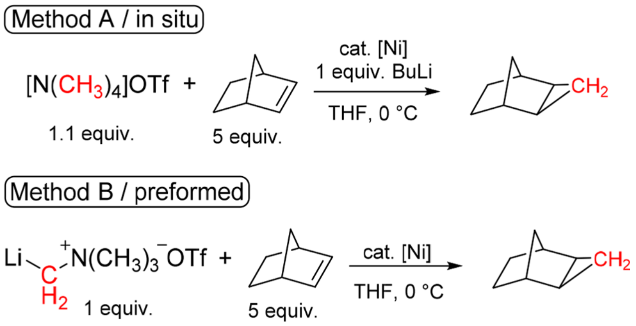

For the kinetic isotope effect calculations, we employed the ISOEFF software, which calculates isotope effects based on the Bigeleisen equation, using input from a quantum mechanical calculation (i.e., the Hessian matrix obtained from Gaussian).[8]

3. RESULTS

Our earlier published work reported yields for cyclopropanation over a limited range of conditions and substrates. In the present report, we extend the experimental data with measurements of rates for cyclopropanation or homocoupling.

3.1. Kinetic Orders. The limited scope and most of the unusual features observed for the reaction had been explained by means of the catalytic cycle depicted in Scheme 1, in particular via the competition between a productive cyclopropanation that would be kinetically first-order in nickel carbene and an unproductive homocoupling that would be second-order in the same carbene. Addition of NMe_3 (up to 1 equiv with respect to ylide) as reported earlier (to test for reversible nickel carbene formation),[4] as well as NMe_2Bn (10 equiv, this report), paradoxically did not improve the cyclopropanation yield or produce a rearrangement product from a putative NMe_2Bn derived ylide (Schemes S17 and S18).[9] This motivated us to execute kinetic experiments—measuring rates as opposed to yields—to confirm or call into question the putative catalytic cycle in Scheme 1.

We used three different methods for preparation of the active Ni(0) species: (a) reduction of Ni(II) in situ prior to ylide formation, (b) reduction of Ni(II) in situ with the ylide, and (c) initiation with a Ni(0) catalyst. The plot of k_{obs} for cyclopropanation of norbornene (the best substrate) versus catalyst loading between 0.25 and 1.0 mol % shows kinetic orders between 0.80 ± 0.02 and 1.17 ± 0.08, as depicted in Figure 1.

We attribute the non-overlapping lines for the three initiation methods to slightly different initiation efficiencies, but we note that all methods deliver close to first-order dependence of cyclopropanation rate on Ni concentration. The initiation method with $Ni(PPh_3)_4$, the Ni(0) source, gave the cleanest first-order kinetics, as well as the highest absolute rates, implying the most efficient activation. Thus, we used the $Ni(PPh_3)_4$ catalyst for the determination of the kinetic order of homocoupling with respect to Ni concentration. For this latter experiment, the consumption of ylide, determined by

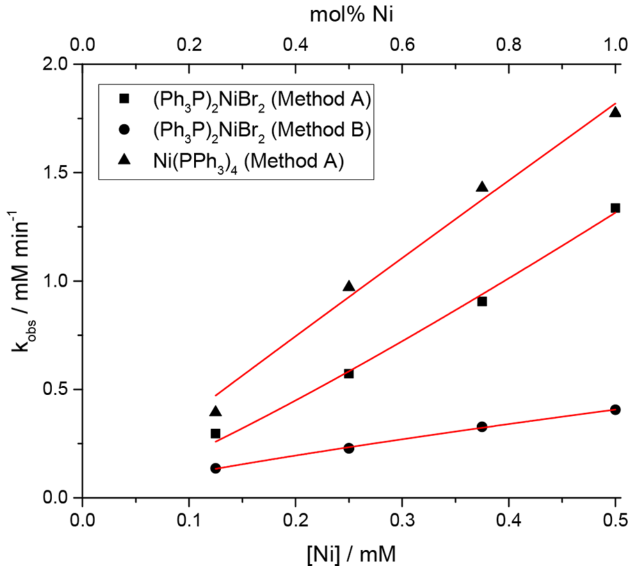

Figure 1. Plot of k_{obs} versus [catalyst] using $(Ph_3P)_2NiBr_2$ and Method A (squares) or Method B (circles) as precatalyst or $Ni(PPh_3)_4$ (Method A, triangles) with NBE. The red curves depict a fit to the function $y = ax^b$ to establish the order in [Ni] as follows: $b = 1.17 \pm 0.08$ (squares), $b = 0.80 \pm 0.02$ (circles), $b = 1.0 \pm 0.1$ (triangles).

quenching of aliquots taken of a reaction set up substrate-free, but otherwise identical to the cyclopropanation runs with preformed ylide (method B), was performed by tracking tetramethylammonium disappearance by ^{1}H NMR, as described in the SI. The plot of k_{obs}, shown in Figure 2, covering the range of catalyst concentration from 0.5 to 2.0 mol %, gave an order of 1.34 ± 0.01 in catalyst, which is closer to first than it is to the second-order behavior that we had expected.

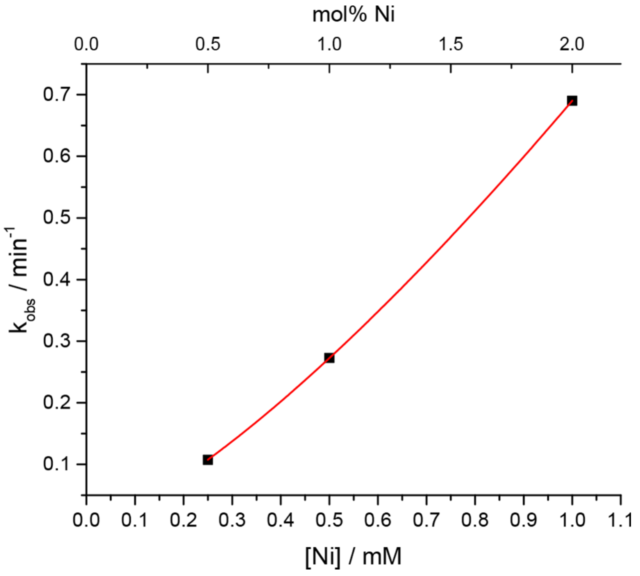

Figure 2. Plot of $[Ni(PPh_3)_4]$ versus k_{obs} for the consumption of ylide in the absence of alkene. The red curve depicts a fit to the function $y = ax^b$ to establish the order in [Ni], $b = 1.34 \pm 0.01$.

The unexpected results with excess trimethylamine[4] and, particularly, the unexpected kinetic order for homocoupling in the absence of substrate, motivated us to determine the kinetic order of the reaction with respect to substrate and phosphine, namely, norbornene and triphenylphosphine. The plots of k_{obs} for cyclopropanation of norbornene versus concentration of either norbornene or triphenylphosphine, shown in Figures 3 and 4, show orders of 0.18 ± 0.02 and 0.17 ± 0.05, respectively, over an approximately one order of magnitude range of concentrations. While the proposed catalytic cycle in Scheme 1 could afford a variety of kinetic orders, depending on which step is rate-limiting, the close to zero-order kinetics with

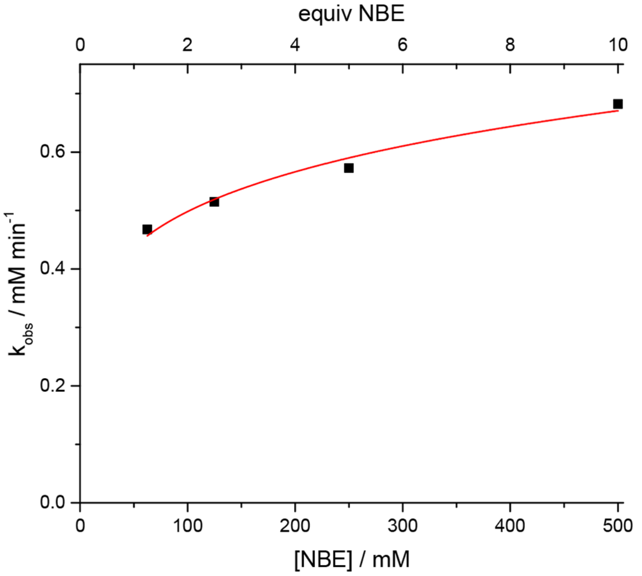

Figure 3. Plot of k_{obs} versus [NBE] using 0.5 mol % $(Ph_3P)_2NiBr_2$ (Method A). The red curve depicts a fit to the function $y = ax^b$ to establish the order in norbornene, $b = 0.18 \pm 0.02$.

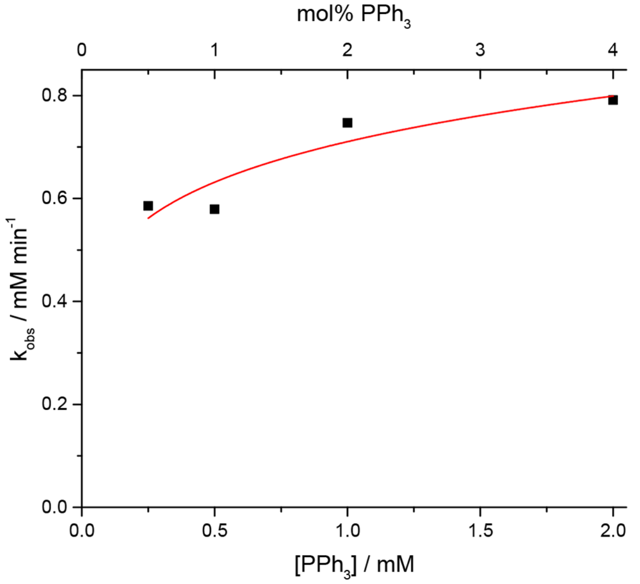

Figure 4. Plot of k_{obs} versus $[PPh_3]$ using 0.5 mol % $Ni(acac)_2$ (Method A). The red curve depicts a fit to the function $y = ax^b$ to establish the order in PPh_3, $b = 0.17 \pm 0.05$.

respect to both substrate and phosphine were nevertheless surprising.

The order in ylide shows a more complex behavior and appears to be 0 or 1 depending on the exact reaction conditions and conversion. An additional discussion about the order in ylide can be found in the Supporting Information (Figure S11).

3.2. Kinetic Isotope Effect. While not entirely foolproof, kinetic isotope effects generally deliver information on the rate-limiting transition state, which makes them appropriate for the present situation. Switching to the perdeuterated ammonium salt $[N(CD_3)_4]OTf$ under otherwise identical conditions (using method A) yielded a large secondary kinetic isotope effect of 2.1 (Scheme 3). This is consistent with sp^3- to sp^2-rehybridization in the rate-limiting transition state, which suggests that the transition state from the Ni-coordinated ylide to the Ni carbene is rate-limiting.

Scheme 3. Determination of a Secondary KIE Using Perdeuterated Tetramethylammonium Triflate

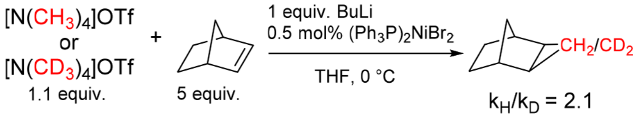

Having the measured k_H/k_D of 2.1, we computationally investigated a number of catalytic cycles to see whether other elementary steps, other than the carbene formation, could plausibly be consistent with the KIE. For each step in a composite catalytic cycle, shown in the SI (Figure S78), we employed the ISOEFF software, which calculates isotope effects based on the Bigeleisen equation, using input from a quantum mechanical calculation (i.e., the Hessian matrix obtained from Gaussian), and found a predicted kinetic isotope effect of $k_H/k_D = 2.50$ for the carbene formation step. No other elementary step gives a KIE even close to compatible with that which we observed experimentally (Table S24).

3.3. Relative Rates of Cyclopropanation for Different Substrates. Given that norbornene provides significantly higher yields, and, accordingly, better mass balances, than the other olefinic substrates tested, we opted, for the determination of rate constants for the cyclopropanation of cyclooctene and 1-octene, for example, for a competition experiment. Binary mixtures of norbornene with the other olefins were cyclopropanated, and the ratio of product cyclopropanes was determined by GC-FID of quenched aliquots, giving the results shown in Figure 5. Adjusting the product ratios for the ratio of the substrates, we obtained the relative rate constants for cyclopropanation of the cyclooctene and 1-octene, relative to that for norbornene, shown in Table 1 (see Discussion).

3.4. Further Yields and Job Plots. We extended the range of yield measurements considerably, as compared to those in our previous report, concentrating on variations in the catalyst loading, variation of the catalyst itself, the Ni:phosphine ratio, and addition of an excess of PPh_3. These results are given in tabular form in the SI, and appear in Figures 9 and 10 in the Discussion, where they will be used as the test set (see below) to assess the adequacy of the our newly proposed catalytic cycle and the minimal kinetic model derived from that catalytic cycle.

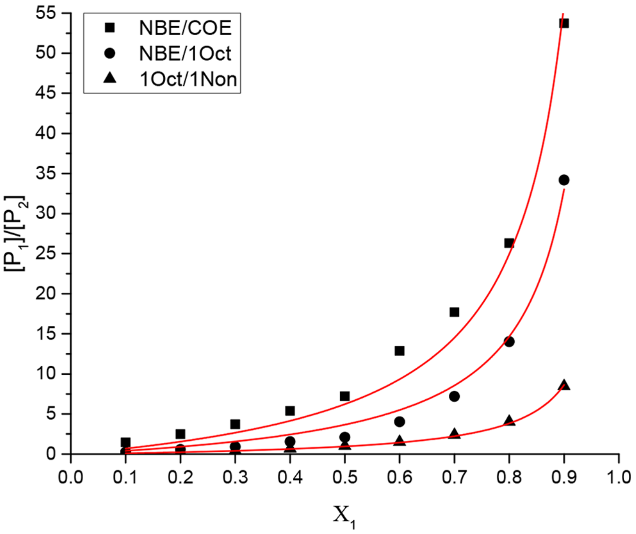

Figure 5. Plot of mole fraction of alkene 1, X_1, versus product ratio, $[P_1]/[P_2]$, derived from alkene 1 and alkene 2, respectively, with the following pairs of alkenes. 1: norbornene, 2: cyclooctene (squares); 1: norbornene, 2:1-octene (circles); 1:1-octene, 2:1-nonene (triangles). 0.5 mol % $(Ph_3P)_2NiBr_2$ was used as precatalyst. The red curves depict a fit to the function $y = aX_1/(1 - X_1)$ (see eq 1 and Discussion). $a = 6.2 \pm 0.2$ (squares), $a = 3.7 \pm 0.1$ (circles), $a = 0.96 \pm 0.01$ (triangles).

4. DISCUSSION

In the following, we discuss the results of our mechanistic studies and how they change and strengthen our understanding of the reaction mechanism at hand.

Mirroring the general structure of the Results section, we look first at the kinetic orders to establish the resting state of the catalyst and discuss the KIE, in order to infer the rate-limiting step. On the basis of these data, we then propose a catalytic cycle. At its heart is a pre-equilibrium between the phosphine ligand(s) and the alkene substrate coordinated to nickel(0) that leads us to propose a Curtin−Hammett-like scenario.

Depending on which side the pre-equilibrium lies, one branch leads to cyclopropanation and the other consumes the ylide in an unproductive side reaction. We develop this scenario into a very simple mathematical model. In order to do so, we first look at the special case of the alkene competition experiments (Figure 5), ignoring the side reaction. Then, we generalize the mathematical formalisms to a single alkene in competition with homocoupling using only one fit parameter.

Finally, we apply this model to our data to shed light on the anomalous observations we made initially.

4.1. Resting State of Catalyst. In our originally proposed catalytic cycle, we assumed that a competition exists between product formation, which is first-order in catalyst, and a background reaction that decomposes the ylide unproductively in a bimolecular homocoupling reaction. This bimolecular homocoupling would be second-order in catalyst, assuming the homocoupling step, whatever its exact nature, to be the rate-limiting step (see below, discussion about KIE).

Contrary to these initial assumptions, we observed the reaction to be approximately first-order in catalyst for the reaction with norbornene, as well as in the absence of any added alkene at all, i.e., when we look at the homocoupling reaction in isolation. Using norbornene as substrate, we

DOI: 10.1021/acs.organomet.9b00027

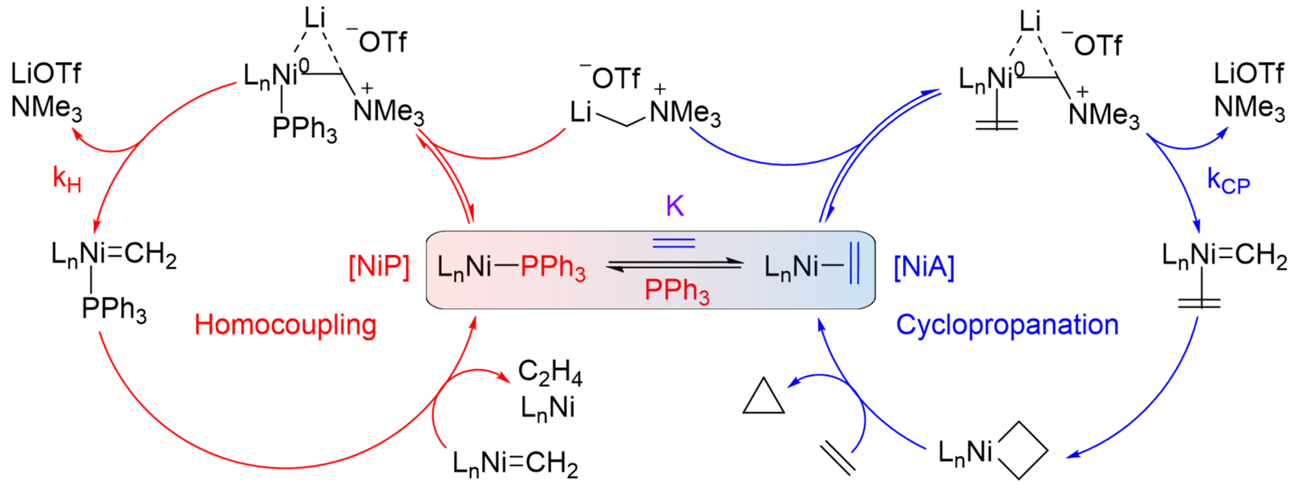

Figure 6. Proposed catalytic cycle. Central to the reaction is the highlighted equilibrium between ligand and alkene binding.

observed approximately zeroth order in olefinic substrate, indicative of saturation behavior in alkene. We also observed a zeroth order in PPh_3 when tracking product formation. Considering these three kinetic orders together, we propose that the resting state is a nickel(0) species with the alkene and/or PPh_3 already coordinated, meaning that substrate coordination has already taken place before the rate-limiting step. Additionally, we argue that the homocoupling reaction has the same resting state manifold and the actual homocoupling step itself is *not* rate-limiting. Thus, product formation and homocoupling intersect via the same resting state manifold of Ni(0) species.

4.2. Rate-Limiting Step. The normal secondary KIE of 2.1 suggests an sp^3- to sp^2-rehybridization in the rate-limiting transition state. This result is most consistent with nickel carbene formation being rate-limiting. Going from the tetrahedral sp^3-hybridized nickel ylide adduct to the planar sp^2-hybridized carbon in the nickel carbene is the only such step in our proposed mechanism.[10] In order to corroborate this finding, we performed DFT calculations on a model system and obtained the KIEs for all relevant steps in our proposed catalytic cycle (Table S24). Indeed, not only is the calculated KIE for the carbene formation in satisfactory agreement with our experimental value but also all other KIEs are close to one or inverse. This corroboration strongly indicates that we correctly identified the turnover-limiting transition state. Additionally, this makes an alternative mechanism, a nucleophilic attack on the nickel-bound alkene by the ylide, followed by ring-closure, unlikely.[11] None of the steps in the alternative mechanism involve a change in hybridization of the appropriate carbon, and thus no (large) KIE would be expected.

Furthermore, the carbene formation by extrusion of NMe_3 can be seen (formally) as an oxidative process, where the niccolate(0) is oxidized to a nickel(II) carbene.[12] This is in agreement with the description of Hillhouse's isolated carbene complexes and selectivities for polar olefins with diazomethane as observed by Ibers.[2c] This picture is corroborated by our calculations, which show that the barrier for NMe_3 extrusion is lowered in a system with more strongly σ-donating ligands, e.g. two PH_3 ligands, than in a system with a less electron-rich nickel center ligated by one phosphine and one ethene (9 versus 15 kcal mol^{-1}, Tables S21 and S25).

4.3. Proposed Catalytic Cycle. Combining the insights presented above regarding the resting state and the rate-limiting step, we propose the catalytic cycle presented in Figure 6. The aforementioned pre-equilibrium in which PPh_3 and alkene compete for nickel(0) is denoted with the equilibrium constant *K* in Figure 6 in the colored block in the center of the diagram. This mechanistic conclusion led us to Tolman's work on the binding affinity of alkenes to nickel(0), specifically nickel(0)-tri-*o*-tolyl phosphite complexes, in which norbornene (K = 4.4) was shown to bind significantly more strongly to nickel(0) than, e.g., cyclooctene (K = 0.062) (Scheme 4).[13]

Scheme 4. Tolman's Alkene Equilibrium Constants[13a]

$$A + NiL_3 \underset{}{\overset{K}{\rightleftharpoons}} (A)NiL_2 + L$$

A = Alkene
L = [P(O-*o*-tolyl)$_3$]

$$K = \frac{[(A)NiL_2][L]}{[NiL_3][A]}$$

Alkene	K^a
Norbornene	4.4
1-Hexene^b	5.0 x 10^{-1}
Cyclooctene	6.2 x 10^{-2}
Cyclohexene	3.5 x 10^{-4}

^{a}Taken from ref. 13a. ^{b}Also used for other 1-alkenes.

We had observed that more strongly bound alkenes (based on Tolman's equilibrium constants) resulted in higher yields for the cyclopropanation, which is consistent with the proposed mechanism.[14,15]

The analogous mechanistic scenario was proposed for the (ligandless) Pd-catalyzed cyclopropanation with diazomethane. In a DFT study by Straub, the extrusion of N_2 from diazomethane by an alkene-ligated Pd(0) complex to form a Pd carbene was identified as the most likely rate-determining step, followed by facile intramolecular cyclopropanation of the η^2-bound alkene.[16] Indeed, the improved yields with diazo compounds or α-lithiated sulfones for more π-acidic alkenes were noted previously.[2c,11b,17] After adduct formation of the ammonium ylide with the active catalyst, extrusion of NMe_3 in the rate-limiting step leads to a nickel carbene species. Once

DOI: 10.1021/acs.organomet.9b00027

the nickel carbene is formed, the bound alkene can undergo intramolecular [2+2] addition to the nickelacyclobutane. This is followed by rapid reductive elimination to give the product. The viability of these kinetically invisible steps has been confirmed by our calculations and has been observed for analogous systems as pointed out earlier.[4]

If, on the other hand, no alkene is coordinated at the time the nickel carbene is formed, it can undergo unproductive homocoupling.

4.4. Derivation of a Minimal Model. As discussed above, we derive our model first for the specific case of two competing alkenes (Scheme 5 and Figure 5).

Scheme 5. Simplified Mechanistic Scenario with an Alkene Exchange Equilibrium before Cyclopropanation

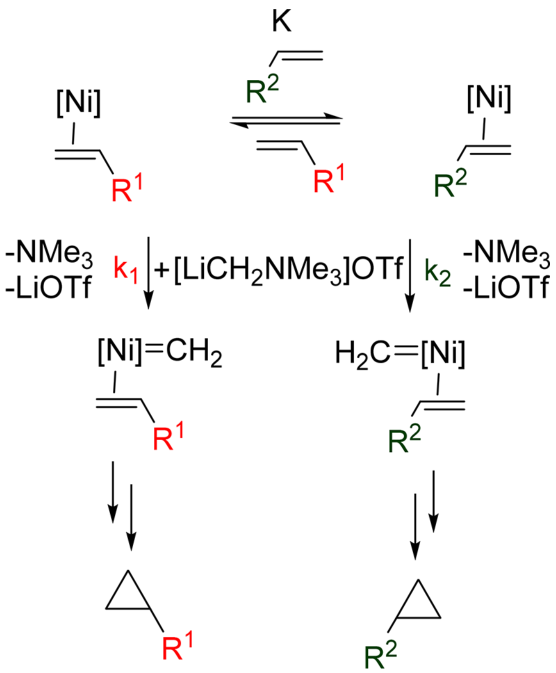

Assuming a Curtin−Hammett scenario, the two alkenes exchange rapidly in a pre-equilibrium (K) *before* the rate-limiting nickel carbene formation (k_1, k_2).[18] This is followed by a fast, irreversible [2+2] cycloaddition once the nickel carbene is formed (i.e., bimolecular alkene exchange is expected to be much slower for the nickel carbene complex compared to unimolecular nickelacyclobutane formation). This simplified mechanistic scenario leads to the following equation for the product ratio derived from alkenes 1 and 2, respectively

$$\frac{[P_1]}{[P_2]} = \frac{k_1K_1}{k_2K_2}\,\frac{X_1}{(1 - X_1)} \qquad (1)$$

where k_i is the rate constant for the cyclopropane formation from the respective nickel alkene complex, K_i corresponds to Tolman's equilibrium constant for alkene i, and X_1 is the mole fraction of alkene 1 (see the Supporting Information for full derivation).[19]

Comparing the fit function from Figure 5, $y = aX_1/(1 - X_1)$, with eq 1 gives $a = k_1K_1/(k_2K_2)$. We then arrive at a relative order of rate constants k_{rel} as seen in Table 1. The competition experiment between 1-octene and 1-nonene serves as an internal validation. The obtained value of $a = 0.96$ is very close to the expected value of 1, indicating that both alkenes behave identically, or at least very similarly (Figure 5).[13a]

Table 1. Determination of Relative Rate Constants from Competition Experiments

alkene	K^a	k_{rel}
Norbornene	4.4	1^c
1-Octene	5.0×10^{-1b}	2.4
Cyclooctene	6.2×10^{-2}	11.4

[a] Values for K are taken from ref 13a. See also discussion in ref 14. [b] Value for 1-hexene in ref 13a. [c] k_{rel} for NBE set to 1.

This model reveals that weakly binding/weaker π-acidic substrates react faster (i.e., k_i (k_{rel}) is larger, less ground state stabilization), but less of the corresponding nickel(0) alkene species is present in solution (K_i is smaller) because they stabilize nickel(0) less.[20] This is logically consistent with an oxidative process (nickel carbene formation) being slower at a less electron-rich metal.

We can now proceed to the more general case in which a single alkene is in a pre-equilibrium with PPh$_3$. The observed first-order kinetics in catalyst for the ylide consumption *in the absence of added alkene* indicates that the nickel carbene formation is also the rate-determining step in the substrate-free case, with an analogous resting state being before that transition state. With this idea in mind, we extend the aforementioned mechanistic model with rapid alkene/alkene exchange before the rate-determining nickel carbene formation, to the general case for the cyclopropanation reaction. This leads to the following mechanistic sketch shown in Scheme 6.

Both pathways, cyclopropanation and unproductive ylide decomposition/homocoupling, share the same resting state manifold, i.e., a nickel(0) species with alkene (NiA) and phosphine ligands (NiP) in equilibrium. If a nickel(0) species with an alkene ligand reacts with an ylide to form the nickel

Scheme 6. Simplified Mechanistic Scenario with an Alkene/Phosphine Exchange Equilibrium before Cyclopropanation

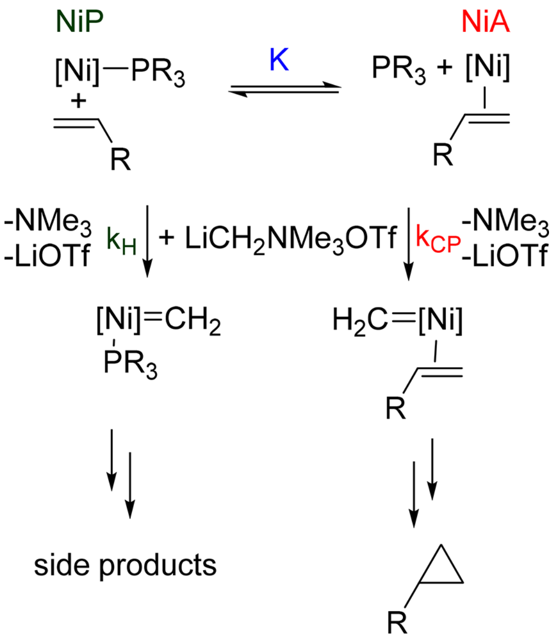

carbene, it will follow the pathway of cyclopropanation (k_{CP}). If, on the other hand, there is no bound alkene but only phosphine ligands on the nickel, it will react unproductively once the nickel carbene is formed (k_H). Both pathways have the same dependence on ylide concentration, (approximately) first-order, as evidenced by the reaction profile of ylide consumption (Figure S12).

This regime leads again to a Curtin–Hammett scenario, where the yield is determined by the competition between the two rates, k_{CP}[ylide][NiA] and k_H[ylide][NiP], with the pre-equilibrium between NiA and NiP controlled by relative concentrations and binding affinities of alkene versus phosphine.

Standard mathematical treatment of this scenario yields the following equation (see the Supporting Information for full derivation)

$$\%\ \text{yield} = 100 \times \frac{\frac{k_{CP}}{k_H}([\text{Ni}]_{tot} - [\text{NiP}])}{\frac{k_{CP}}{k_H}[\text{Ni}]_{tot} + \left(1 - \frac{k_{CP}}{k_H}\right)[\text{NiP}]} \quad (2)$$

where [NiP] is a function of the total concentrations of Ni, phosphine, and alkene, $[\text{Ni}]_{tot}$, $[\text{P}]_{tot}$, and $[\text{A}]_{tot}$, respectively, as well as the equilibrium constant K. The yield is thus dependent on these three concentrations, as well as on the alkene binding constant K and on the ratio of the rate constants k_{CP}/k_H (Scheme 6).

This model can also be applied to the rate of cyclopropanation to give eq 3. In this case, $k_{obs,rel}$ is normalized against an arbitrarily chosen reference k_{obs} of a given series of experimental data (usually the lowest concentration of $[\text{Ni}]_{tot}$).

$$k_{obs} = k_{CP}[\text{NiA}] = k_{CP}([\text{Ni}]_{tot} - [\text{NiP}]) \quad (3)$$

$$k_{obs,rel,n} = \frac{k_{CP}([\text{Ni}]_{tot,n} - [\text{NiP}]_n)}{k_{CP}([\text{Ni}]_{tot,1} - [\text{NiP}]_1)} = \frac{[\text{NiA}]_n}{[\text{NiA}]_1} \quad (4)$$

At this point, we refrain from making any assumptions about what the possible species NiP and NiA might look like, except that NiA is a species with *at least one alkene coordinated*, whereas NiP is a species in which one alkene has been replaced by a phosphine ligand (PPh_3 in this case), most likely however an alkene-free *tris*-phosphine nickel complex.

4.5. Fit of Model to Data.

Next, we apply this mechanistic model to our data to see if it agrees with our observations, at least qualitatively.

Using the model described above, we used the ratio k_{CP}/k_H as the *sole* parameter to fit eq 2 to the cyclopropanation yields with different alkenes (Figure 7) at *one* representative set of concentrations (see Figure S20 for other catalyst concentrations). This gives a ratio of rate constants k_{CP}/k_H of 0.014. That is, the rate *constant* of homocoupling (k_H) is larger than that for cyclopropanation (k_{CP}). Note that k_{CP} is therefore an *average* value over all alkenes. Because the alkene is necessarily involved in the rate-limiting step (according to our model), k_{CP} should vary with the nature of the alkene and thus k_{CP} is not independent of K.

We already gleaned this interdependence of k_{CP} and K in the alkene competition experiments (as k_{rel} in Table 1), but we chose to use the admittedly extreme simplification of a single k_{CP}/k_H ratio and compare the numerical results to experiment.

4.6. Comparison of Model to Data.

The extracted parameter k_{CP}/k_H (Figure 7) is the *sole fit* to our mechanistic data; accordingly, all further predictions are based thereupon.

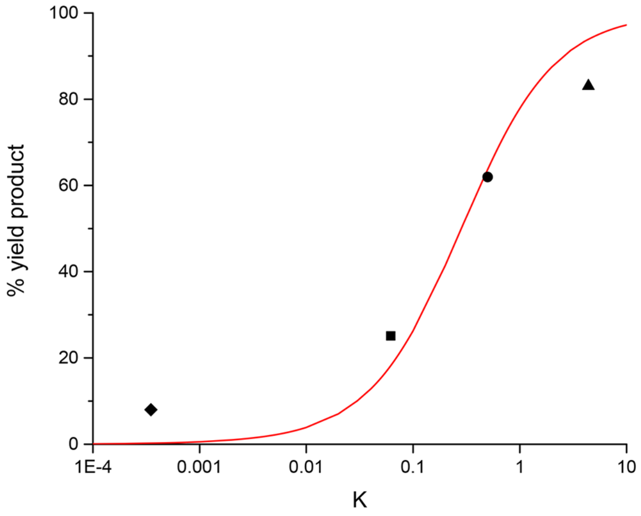

Figure 7. Plot of K (from Tolman,[13] log scale) versus the experimental yield (black symbols, 1.0 mol % $(Ph_3P)_2NiBr_2$) and the predicted yield (red line) based on our mechanistic model for the cyclopropanation of cyclohexene (diamond, data from ref 4), COE (square), 1-octene (circle), and NBE (triangle). The ratio k_{CP}/k_H was used as a parameter to fit the experimental data according to eq 2 to give k_{CP}/k_H = 0.014. $[\text{Ni}]_{tot}$ = 0.5 mM, $[\text{P}]_{tot}$ = 1 mM, $[\text{A}]_{tot}$ = 250 mM.

Figure 8, in which the computed yield for cyclopropanation of cyclooctene over a broad range of substrate concentrations matches the experiment well, despite the fit of k_{CP}/k_H at a single concentration, gives a first indication that this rather bold approximation provides a better-than-qualitative description of the reaction.

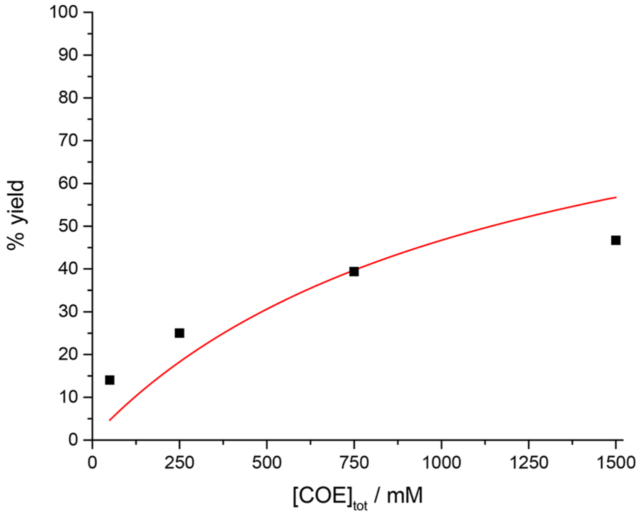

Figure 8. Plot of COE concentration versus the measured yield (squares) and predicted yield (red curve) based on our model (eq 2) for cyclopropanation of COE using 1.0 mol % $(Ph_3P)_2NiBr_2$. k_{CP}/k_H = 0.014, $[\text{Ni}]_{tot}$ = 0.5 mM, $[\text{P}]_{tot}$ = 1 mM with no further adjustment of parameters. Data from ref 4.

In agreement with our rate data above, the model reasonably reproduces the orders in NBE, PPh_3, and catalyst (Figures S24–S26), as would be expected.

The model also predicts that, for NBE as substrate, the rate of cyclopropanation might change significantly but the yield does not vary noticeably, despite there being an exchange of phosphine and olefin in the resting state, as seen in Figure 9.

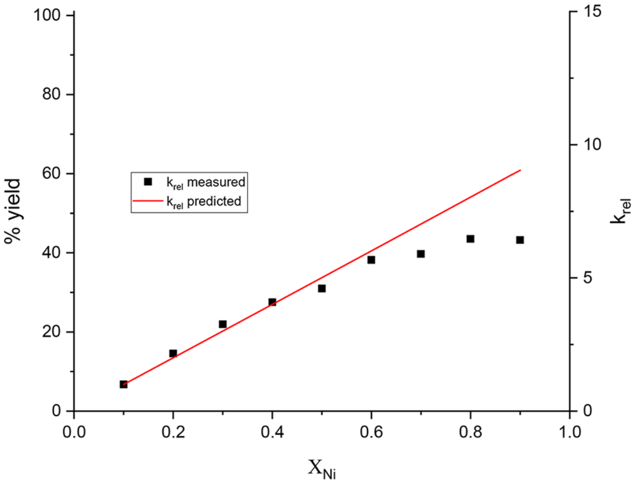

Figure 9. Plot of mole fraction of nickel X_{Ni} (using $Ni(acac)_2$) versus the measured rate (squares) and predicted rate (red solid curve) (approximated as initial yield after 30 min) based on our model (eq 4) for the cyclopropanation of NBE, all with no further adjustment of parameters. $k_{CP}/k_H = 0.014$, $[Ni]_{tot} + [P]_{tot} = 0.5$ mM, $[A]_{tot} = 250$ mM.

At higher X_{Ni}, the experimental yields and rates deviate downward from those predicted by our model. A reasonable explanation for this behavior is a less stable catalyst under the very low concentration of phosphine ligand (Figure 9).

One key initial finding, as mentioned in the Introduction and for which we sought an explanation, was that, at higher catalyst loading, the yield of cyclopropanation is suppressed using COE as substrate. This has been shown here also for norbornene (and 1-octene) as substrate, but only if a Ni(II) precatalyst is used, and only to a small extent in the NBE case. When an already reduced precatalyst, $Ni(PPh_3)_4$, was used the same effect was observed for cyclooctene but not for norbornene (Figure 10). This shows, on the one hand, that the reduction of Ni(II) to Ni(0), as we propose, is an issue and does lead to partial catalyst deactivation. This can also be gleaned from the data in Figure 1.

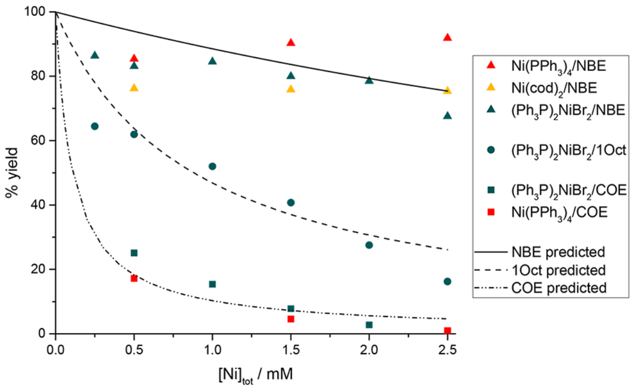

Figure 10. Plot of catalyst concentration versus yield for COE (squares), 1-octene (circles), and norbornene (triangles). The black curves depict the predicted yield based on our model (eq 2), with no further adjustment of parameters. $k_{CP}/k_H = 0.014$, $[P]_{tot} = 2[Ni]_{tot}$, $[A]_{tot} = 250$ mM.

On the other hand, with the model in hand, this catalyst loading effect can be explained by the specific interplay between K for the alkene and the catalyst concentration employed. With increasing precatalyst loading, there is a simultaneous increased concentration of phosphine ligand (P_{tot}) in the system, while the concentration of alkene (A_{tot}) is kept constant. On the basis of the value of K, it is possible for the phosphine ligand to replace the alkene binding to the catalyst; i.e., [NiP] increases and more ylide decomposes unproductively in a parasitic side reaction. Thus, the observed decrease in yield is not present for a strongly binding alkene (NBE) but is observable for a weakly binding alkene (COE) (Figure 10). In accordance with this model, addition of an excess of PPh_3 under otherwise standard conditions for COE led to a strongly suppressed or even completely inhibited cyclopropanation reaction (see the Supporting Information). This also explains why chelating bisphosphine or strongly binding monophosphine ligands have proven to be worse ligands than PPh_3 in terms of yield. The alkene cannot compete for a coordination site on the metal, leaving the ylide to decompose unproductively. The binding of phosphines to Ni(0) has been shown to be dominated by steric effects.[21] The initial rise in cyclopropanation yield as the Ni concentration is increased is likely explained by outcompeting catalyst decomposition and uncatalyzed ylide decomposition relative to the slow rate of cyclopropanation at low catalyst loadings.

4.7. Implication for Ligand Design. Thus, far, we have only looked at the influence of the alkene substrate on the proposed pre-equilibrium. To make the reaction catalyst-controlled, guided by our mechanistic insight, a catalyst/ligand system is needed that does not inhibit, or even promotes, binding of the substrate, yet still has an ancillary ligand to stabilize Ni(0). We took inspiration from a recent report by Wu and Doyle regarding the influence of remote steric effects.[22] A small buried volume $\%V_{Bur}$ of a phosphine ligand would allow for substrate coordination. A large cone angle with substituents pointing away from the immediate coordination sphere of Ni would nevertheless result in a large steric profile with respect to coordination of more than one phosphine.

With this rationale in mind, we synthesized two new triaryl phosphine ligands with differing numbers of 3,5-di-*tert*-butylphenyl groups on phosphorus, either one or two. Indeed, both ligands gave improved yields over the standard ligand PPh_3 for the cyclopropanation of COE, 32% and 48%, respectively (Figure 11 and Table S18).

To test our hypothesis of the remote steric effect, we generated a steric-only regression model using five different phosphines ranging from the sterically small $PPhMe_2$ to our new, larger ligands (as well as spanning the largest range of yields presently possible for the substrate COE).[23] We generated for the ligand set two steric parameters, buried volume $\%V_{Bur}$ and exact ligand solid cone angle $\Theta°$.[24]

Already a good correlation between predicted and measured yields for our small ligand set can be achieved using only these two steric parameters, displaying the merit of harnessing remote steric effects on the ligand design. Additionally, the applicability of our rationale is reflected in the coefficients extracted from the regression model (Figure 11); i.e., the larger the cone angle with concomitantly small buried volume, the higher the predicted yield.

To further assess the veracity of the implicated pre-equilibrium binding, we measured the binding constants K for cyclooctene in the presence of the ligands in Figure 11 (see

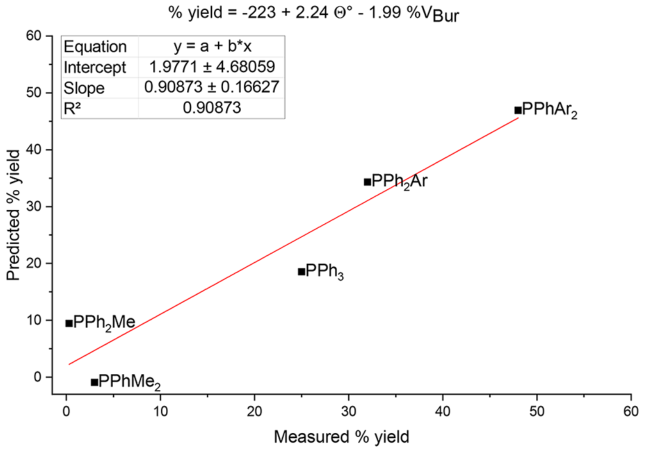

Figure 11. Plot of measured yield versus predicted yield using a steric-only regression model with buried volume $\%V_{\text{Bur}}$ and exact solid cone angles Θ°. Ar = (3,5-di-^{t}BuPh).

the Supporting Information). Indeed, the K correlates well with the cyclopropanation yield. Figure 7 has been reproduced in the Supporting Information with the additional data (Figure S76).

5. CONCLUSION

In summary, our mechanistic studies lead us to propose a kinetic model that explains (most) experimental observations, at least qualitatively, and gave us initial guidelines for an improved, and partially verified, rational ligand design.

(1) The active nickel catalyst with at least one alkene bound, NiA, is the resting state of the catalytic (cyclopropanation) cycle. The concentration of NiA, in turn, depends on the equilibrium constant K; for NBE, the concentration of NiA is higher than for COE. This species can undergo nickel carbene formation with the ammonium ylide present in solution, followed by rapid product formation, most likely via a nickelacyclobutane.

(2) Depending on the binding constant K of the alkene substrate, a significant amount of the nickel catalyst can exist as an alkene-free nickel species (NiP) that can also undergo nickel carbene formation in the rate-determining step to engage in rapid homocoupling (and, potentially, further side reactions) (highlighted equilibrium in Figure 6). We propose NiP to be the resting state of this side-reaction cycle.

(3) Carbene formation is faster for NiP than NiA ($k_{\text{H}} > k_{\text{CP}}$, Figure 7). Thus, NiP competes for the ylide in a parasitic cycle. This explains the pronounced substrate dependence of the yield that we noted earlier. Unless the substrate binds well enough to drive the equilibrium to the alkene-ligated nickel species, and, therefore, cyclopropanation, the phosphine-ligated species will dominate and engage in the faster and unproductive background reaction, i.e., homocoupling (Figure 6).

(4) Additionally, competition experiments indicate that there is an inverse relationship between the equilibrium constant K and the rate constant k_{CP} for cyclopropanation (i.e., k_{rel} in Table 1). Together with the larger rate constant for homocoupling k_{H} over the (average) rate constant for cyclopropanation k_{CP} (Figure 7), one can see that the higher the π-acidity of the ligand is (NBE > PPh_3), the smaller the rate constant becomes.

(5) The product of the homocoupling, ethene, is also itself an outstanding ligand.[13] A headspace analysis of the reaction showed that cyclopropane is a side product of the reaction. Leaving the flask open to the Schlenk line likely allows the ethene to escape and thus might be the reason for the effect of an open versus a closed reaction flask.

(6) Our mechanistic studies have afforded us with a blueprint for an improved ligand design. The pre-equilibrium binding can be influenced by employing ligands with remote steric hindrance, expressed as a small buried volume and a large cone angle, thus discouraging saturation of the catalyst with phosphine ligands, i.e., resulting in a larger K. Our measured binding constants for several phosphines give credence to this hypothesis.

The above-outlined mechanism and the resulting blueprint for an improved ligand design will serve as a highly valuable basis for the rational design of new ligands with the above-mentioned features. Our initial results showcase a promising way forward. These mechanism-driven efforts, including an enlarged and more detailed ligand parametrization set, are currently ongoing and will be reported in due course.

■ ASSOCIATED CONTENT

Ⓢ Supporting Information

The Supporting Information is available free of charge on the ACS Publications website at DOI: 10.1021/acs.organomet.9b00027.

Experimental details, characterizations, and geometries for all computed structures (PDF)
Cartesian coordinates (XYZ)

■ AUTHOR INFORMATION

Corresponding Author

*E-mail: peter.chen@org.chem.ethz.ch.

ORCID

Renana Gershoni-Poranne: 0000-0002-2233-6854
Peter Chen: 0000-0002-9280-4369

Funding

This work was supported by the Schweizerischen Nationalfonds and the ETH Zürich.

Notes

The authors declare no competing financial interest.

■ ACKNOWLEDGMENTS

Augustin A. S. W. Tchawou (Chen group) is thanked for the preparation of authentic heptylcyclopropane and its GC calibration curve.

■ REFERENCES

(1) (a) Pasco, M.; Gilboa, N.; Mejuch, T.; Marek, I. The Renaissance of Zinc Carbenoid in Stereoselective Synthesis in Acyclic Systems. *Organometallics* **2013**, *32*, 942−950. (b) Charette, A. B. Cyclopropanation mediated by zinc organometallics. In *The Chemistry of Organozinc Compounds*; Rappoport, Z., Marek, I., Eds.; Wiley: Chichester, U.K., 2006; Vol. *1*, pp 237−286. For a recent Ni-catalyzed Simmons−Smith-type method, see: (c) Zhou, Y.-Y.; Uyeda, C. Reductive Cyclopropanations Catalyzed by Dinuclear Nickel Complexes. *Angew. Chem., Int. Ed.* **2016**, *55*, 3171−3175.

(2) (a) Tomilov, Y. V.; Bordakov, V. G.; Dolgii, I. E.; Nefedov, O. M. Reaction of diazoalkanes with unsaturated compounds.

Communication 2. Cyclopropanation of olefins by diazomethane in the presence of palladium compounds. *Bull. Acad. Sci. USSR, Div. Chem. Sci.* **1984**, *33*, 533−538. (b) Denmark, S. E.; Stavenger, R. A.; Faucher, A.-M.; Edwards, J. P. Cyclopropanation with Diazomethane and Bis(oxazoline)palladium(II) Complexes. *J. Org. Chem.* **1997**, *62*, 3375−3389. (c) Nakamura, A.; Yoshida, T.; Cowie, M.; Otsuka, S.; Ibers, J. A. Cyclopropanation Reactions of Diazoalkanes with Substituted Olefins in the Presence and Absence of Nickel(0) and Palladium(0) Catalysts. The Structure of (Diazofluorene)bis(*tert*-butyl isocyanide)nickel(0); a Complex Containing a π-Bonded Diazofluorene Molecule. *J. Am. Chem. Soc.* **1977**, *99*, 2108−2117.

(3) (a) Tchawou, A. S. W.; Raducan, M.; Chen, P. Mechanism-Based Design and Optimization of a Catalytic Electrophilic Cyclopropanation without Diazomethane. *Organometallics* **2017**, *36*, 180−191. (b) den Hartog, T.; Sarria Toro, J. M.; Chen, P. A Palladium-Catalyzed Methylenation of Olefins Using Halomethylboronate Reagents. *Org. Lett.* **2014**, *16*, 1100−1103. (c) Morandi, B.; Carreira, E. M. Iron-Catalyzed Cyclopropanation in 6 M KOH with in Situ Generation of Diazomethane. *Science* **2012**, *335*, 1471−1474. (d) Gai, Y.; Julia, M.; Verpeaux, J.-N. Nickel-Catalyzed Cyclopropanation of Alkenes via Methylene Transfer from Lithiated *tert*-Butyl Methyl Sulfone. *Synlett* **1991**, *1991*, 56−57.

(4) Künzi, S. A.; Sarria Toro, J. M.; den Hartog, T.; Chen, P. Nickel-Catalyzed Cyclopropanation with NMe$_4$OTf and *n*BuLi. *Angew. Chem., Int. Ed.* **2015**, *54*, 10670−10674.

(5) We have made this observation for both the Ni-catalyzed reaction in ref 4 as well as the uncatalyzed reaction in refs 10b and 15.

(6) All attempts to isolate a nickel carbene in analogy to Hillhouse's complexes derived from an ammonium ylide have failed so far. See: (a) Mindiola, D. J.; Hillhouse, G. L. Synthesis, Structure, and Reactions of a Three-Coordinate Nickel-Carbene Complex, {1,2-Bis(di-*tert*-butylphosphino)ethane}Ni=CPh$_2$. *J. Am. Chem. Soc.* **2002**, *124*, 9976−9977. (b) Iluc, V. M.; Hillhouse, G. L. Three-Coordinate Nickel Carbene Complexes and Their One-Electron Oxidation Products. *J. Am. Chem. Soc.* **2014**, *136*, 6479−6488.

(7) Frisch, M. J.; Trucks, G. W.; Schlegel, H. B.; Scuseria, G. E.; Robb, M. A.; Cheeseman, J. R.; Scalmani, G.; Barone, V.; Petersson, G. A.; Nakatsuji, H.; Li, X.; Caricato, M.; Marenich, A.; Bloino, J.; Janesko, B. G.; Gomperts, R.; Mennucci, B.; Hratchian, H. P.; Ortiz, J. V.; Izmaylov, A. F.; Sonnenberg, J. L.; Williams-Young, D.; Ding, F.; Lipparini, F.; Egidi, F.; Goings, J.; Peng, B.; Petrone, A.; Henderson, T.; Ranasinghe, D.; Zakrzewski, V. G.; Gao, J.; Rega, N.; Zheng, G.; Liang, W.; Hada, M.; Ehara, M.; Toyota, K.; Fukuda, R.; Hasegawa, J.; Ishida, M.; Nakajima, T.; Honda, Y.; Kitao, O.; Nakai, H.; Vreven, T.; Throssell, K.; Montgomery, J. A., Jr.; Peralta, J. E.; Ogliaro, F.; Bearpark, M.; Heyd, J. J.; Brothers, E.; Kudin, K. N.; Staroverov, V. N.; Keith, T.; Kobayashi, R.; Normand, J.; Raghavachari, K.; Rendell, A.; Burant, J. C.; Iyengar, S. S.; Tomasi, J.; Cossi, M.; Millam, J. M.; Klene, M.; Adamo, C.; Cammi, R.; Ochterski, J. W.; Martin, R. L.; Morokuma, K.; Farkas, O.; Foresman, J. B; Fox, D. J. *Gaussian 09*, Revision D.01; Gaussian, Inc.: Wallingford, CT, 2016.

(8) Anisimov, V.; Paneth, P. ISOEFF98. A program for studies of isotope effects using Hessian modifications. *J. Math. Chem.* **1999**, *26*, 75−86.

(9) The ammonium ylide derived from deprotonating [BnNMe$_3$]X is known to undergo facile Stevens and Sommelet−Hauser rearrangements and did so under our conditions (BuLi, THF, 0 °C, no [Ni] or alkene present). (a) Stevens, T. S.; Creighton, E. M.; Gordon, A. B.; MacNicol, M. CCCCXXIII.-Degradation of Quaternary Ammonium Salts. Part I. *J. Chem. Soc.* **1928**, *0*, 3193−3197. (b) Puterbaugh, W. H.; Hauser, C. R. Isolation of Intermediate Alkali Salt in *ortho*-Substitution Rearrangement of Benzyltrimethylammonium Ion as Benzophenone Adduct. *J. Am. Chem. Soc.* **1964**, *86*, 1105−1107. (c) Lepley, A. R.; Becker, R. H. Quaternary benzylammonium ion rearrangements with organolithium compounds-I: Simple tertiary amines from the attack of N-butyl-lithium on benzyltrimethylammonium iodide. *Tetrahedron* **1965**, *21*, 2365−2373.

(10) (a) On the basis of X-ray crytal structure of the complex [(Cy$_3$PCH(CH$_3$)Ni(CO)$_3$], it has been noted that the phosphonium ylide carbon is sp^3-hybridized: Heydenreich, F.; Mollbach, A.; Wilke, G.; Dreeskamp, H.; Hoffmann, E. G.; Schroth, G.; Seevogel, K.; Stempfle, W. Stevensanaloge, Durch Nickelkomplexe Katalysierte Umlagerung Von Triarylphosphoryliden Und Darstellung Sowie Strukturbestimmung Von Phosphorylid-Nickeltricarbonylkomplexen. *Isr. J. Chem.* **1972**, *10*, 293−319. (b) Additionally, computational studies by our group have shown that the anionic carbon of the N-ylide is tetrahedral with or without coordination to Li: den Hartog, T.; Sarria Toro, J. M.; Couzijn, E. P. A.; Chen, P. A lithiomethyl trimethylammonium reagent as a methylene donor. *Chem. Commun.* **2014**, *50*, 10604−10607.

(11) This mechanistic possibility has been proposed with diazomethane via an outer sphere attack or with an α-lithiated sulfone via coordination/insertion, respectively: (a) Harrold, N. D.; Corcos, A. R.; Hillhouse, G. L. Synthesis, structures, and catalytic reactivity of bis(N-heterocyclic carbene) supported diphenyldiazomethane and 1-azidoadamantane complexes of nickel. *J. Organomet. Chem.* **2016**, *813*, 46−54. (b) Gai, Y.; Julia, M.; Verpeaux, J.-N. Conversion of non-activated alkenes into cyclopropanes with lithiated sulfones under nickel catalysis. *Bull. Soc. Chim. Fr.* **1996**, *133*, 817−829.

(12) Concomitantly, the oxidation state of the transferred carbon atom changes from −2 to −4 going from the ylidic carbon to the carbenic carbon. Formally, this process can be regarded a reductive cleavage of the C−N bond.

(13) (a) Tolman, C. A. Olefin Complexes of Nickel(0). III. Formation Constants of (Olefin)bis(tri-*o*-tolyl phosphite)nickel Complexes. *J. Am. Chem. Soc.* **1974**, *96*, 2780−2789. (b) The analogous equilibrium constant for Ni(PPh$_3$)$_3$ and ethene has also been measured and is comparable to the value with P(O-*o*-tolyl)$_3$) from ref 13a, K = 250 (ref 13a.) vs 300 (ref 13c): (c) Tolman, C. A.; Seidel, W. C.; Gerlach, D. H. Triarylphosphine and Ethylene Complexes of Zerovalent Nickel, Palladium, and Platinum. *J. Am. Chem. Soc.* **1972**, *94*, 2669−2676.

(14) While the equilibrium constants measured in ref 13a were determined under different conditions (benzene at room temperature with P(O-*o*-tolyl)$_3$) than our reaction conditions (THF at 0 °C with PPh$_3$), the *qualitative trend* should be the same. We opted for these experimental values to already have a large library of alkenes at hand. Additionally, we measured the binding constants for cyclooctene, 1-octene, and norbornene with PPh$_3$ (THF, room temperature) and cyclooctene with P(O-*o*-tolyl)$_3$ with a good agreement to Tolman's values (see the Supporting Information, Table S8).

(15) Other (activated) alkenes with equilibrium constants K greater than that of norbornene (see ref 13a) can already react with [LiCH$_2$N(CH$_3$)$_3$]OTf in an uncatalyzed addition-ring-closure sequence to give cyclopropanes (e.g., styrene (K = 10, ref 13a); see: Sarria Toro, J. M.; den Hartog, T.; Chen, P. Cyclopropanation of styrenes and stilbenes using lithiomethyl trimethylammonium triflate as methylene donor. *Chem. Commun.* **2014**, *50*, 10608−10610.

(16) (a) Straub, B. Pd(0) Mechanism of Palladium-Catalyzed Cyclopropanation of Alkenes by CH$_2$N$_2$: A DFT Study. *J. Am. Chem. Soc.* **2002**, *124*, 14195−14201. (b) For a computational study for cyclopropanation with a Ni carbene, see: Zhang, X.; Geng, Z.-Y.; Wang, Y.-C.; Li, W.-Q.; Wang, Z.; Liu, F.-X. A theoretical study nickel-catalyzed cyclopropanation reactions. Nickel(0) versus nickel(II). *J. Mol. Struct.: THEOCHEM* **2009**, *893*, 56−66.

(17) (a) Anciaux, A. J.; Hubert, A. J.; Noels, A. F.; Petiniot, N.; Teyssié, P. Transition-Metal-Catalyzed Reactions of Diazo Compounds. 1. Cyclopropanation of Double Bonds. *J. Org. Chem.* **1980**, *45*, 695−702. (b) Berthon-Gelloz, G.; Marchant, M.; Straub, B.; Marko, I. E. Palladium-Catalyzed Cyclopropanation of Alkenyl Silanes by Diazoalkanes: Evidence for a Pd^0 Mechanism. *Chem. - Eur. J.* **2009**, *15*, 2923−2931.

(18) This sccenario is not unsimilar to the hydrogenation (under low H$_2$ pressure) of acetamidocinnamate with a cationic Rh(I) catalyst, where the product ratio (enantiomeric excess) depends on both the binding pre-equilibrium of the substrate and the subsequent turnover-limiting step: Landis, C. R.; Halpern, J. Asymmetric Hydrogenation of Methyl-(Z)-α-acetamidocinnamate Catalyzed by

{1,2-Bis((phenyl-*o*-anisoyl)phosphino)ethane}rhodium(I): Kinetics, Mechanism, and Origin of Enantioselection. *J. Am. Chem. Soc.* **1987**, *109*, 1746−1754.

(19) Using the equilibrium constants from ref 13a, we simplify our analysis by comparing the relative stabilities of the nickel alkene complexes with respect to the (hypothetical) reference compound of Ni(P(O-*o*-tolyl)$_3$)$_3$.

(20) ESCA Ni $^2P_{3/2}$ binding energies for (alkene)Ni(P(O-*o*-tolyl)$_3$)$_2$ correlate with their formation constants K from ref 13a. Also, homoleptic phosphine/phosphite complexes of nickel(0) have lower Ni $^2P_{3/2}$ binding energies than their monoalkene counterparts. For ESCA data, see: Tolman, C. A.; Riggs, W. M.; Linn, W. J.; King, C. M.; Wendt, R. C. Electron Spectroscopy for Chemical Analysis of Nickel Compounds. *Inorg. Chem.* **1973**, *12*, 2770−2778.

(21) All bisphosphine ligands employed gave ≤12% yield for the cyclopropanation of COE (23% with $(Ph_3P)_2NiBr_2$); see ref 4. Tolman has shown that coordination of (mono)phosphines to Ni(0) is largely dominated by sterics and smaller cone angles result in more stable complexes. In our case, this resulted in the following trend (ref 4): PPh_3 (145°, 23%), PPh_2Me (136°, <1%), $PPhMe_2$ (122°, 3%), PBu_3 (132°, 11%). (a) Tolman, C. A. Phosphorus Ligand Exchange Equilibria on Zerovalent Nickel. A Dominant Role for Steric Effects. *J. Am. Chem. Soc.* **1970**, *92*, 2956−2965. (b) Tolman, C. A.; Reutter, D. W.; Seidel, W. C. A Calorimetric study of steric effects in the reactions of phosphorus ligands with Ni(COD)$_2$. *J. Organomet. Chem.* **1976**, *117*, C30−C33.

(22) Wu, K.; Doyle, A. G. Parametrization of phosphine ligands demonstrates enhancement of nickel catalysis via remote steric effects. *Nat. Chem.* **2017**, *9*, 779−784.

(23) For two recent examples for the parametrization of phosphine ligands in catalysis, see: (a) Reference 22. (b) Zhao, S.; Gensch, T.; Murray, B.; Niemeyer, Z. L.; Sigman, M. S.; Biscoe, M. R. Enantiodivergent Pd-catalyzed C-C bond formation enabled through ligand parametrization. *Science* **2018**, *362*, 670−674.

(24) (a) Falivene, L.; Credendino, R.; Poater, A.; Petta, A.; Serra, L.; Oliva, R.; Scarano, V.; Cavallo, L. SambVca 2. A Web Tool for Analyzing Catalytic Pockets with Topographic Steric Maps. *Organometallics* **2016**, *35*, 2286−2293. (b) Bilbrey, J. A.; Kazez, A. H.; Locklin, J.; Allen, W. D. Exact Ligand Solid Angles. *J. Chem. Theory Comput.* **2013**, *9*, 5734−5744.

DOI: 10.1021/acs.organomet.9b00027